RAPID COMMUNICATIONS

PHYSICAL REVIEW B VOLUME 51, NUMBER 8 15 FEBRUARY 1995-II

Quantum-dot ground states in a magnetic field studied by single-electron tunneling spectroscopy on double-barrier heterostructures

T. Schmidt, M. Tewordt,* R. H. Blick, R. J. Haug, D. Pfannkuche, and K. v. Klitzing
Max-Planck-Institut für Festkörperforschung, Heisenbergstrasse 1, 70569 Stuttgart, Germany

A. Förster and H. Lüth
Institut für Schicht- und Ionentechnik, Forschungszentrum Jülich, Postfach 1913, 52425 Jülich, Germany
(Received 1 December 1994)

The few-electron ground states of a strongly asymmetric nanometer-scale $Al_xGa_{1-x}As$-GaAs double-barrier quantum dot are probed by single-electron tunneling spectroscopy. Magnetotunneling measurements reveal transitions of spin and orbital angular momentum of the two- and three-electron quantum-dot ground states, respectively. The experimental data are compared with exact calculations of the few-electron ground-state energies. Magnetic-field-induced modulations of the tunneling rate in the many-electron regime indicate correlations in the involved states.

Transport through semiconductor quantum dots is dominated by the interplay between size quantization and Coulomb-charging effects, the latter being responsible for single-electron tunneling (SET).[1] Quantum dots containing only a *single* or *few electrons* have been experimentally investigated by employing SET (Refs. 2–4) and single-electron capacitance spectroscopy.[5] The special interest in the few-particle regime arises from the fact that the intradot electron-electron interaction is most important in this case. This impedes a simple independent-particle treatment but allows the exact calculation of the energy states.[6,7]

Here, we report on SET spectroscopy of nanometer-scale laterally confined double-barrier resonant-tunneling structures (DBRTS's) with extremely large degree of barrier-thickness asymmetry. We restrict ourselves to the bias-voltage polarity chosen such that the electrons enter the quantum dot through the thin and leave through the thick barrier, i.e., the charging regime. This favors the observation of *few-electron ground states* while concealing tunneling through excited states. In contrast to earlier work on weakly asymmetric structures,[4] our measurements are, as a consequence of the large asymmetry, not affected by fluctuations of the local density of states in the emitter.

The double-barrier heterostructure used in this study was grown by molecular-beam epitaxy on n^+-type GaAs substrate. The undoped active layers comprise a 10-nm GaAs quantum well, sandwiched between 5-nm and 9-nm $Al_{0.3}Ga_{0.7}As$ top and bottom barriers. Two 300-nm GaAs layers, which are n-doped with Si to 4×10^{17} cm^{-3} and separated from the barriers by 7-nm undoped GaAs spacer layers, provide the top and bottom contacts to the double-barrier structure. Free-standing quantum pillars with AuGe/Ni Ohmic contacts were fabricated from the heterostructure. For processing, we employed optical and electron-beam lithography, reactive-ion etching,[8] and a polyimide insulation technique to support top bonding pads.[2,3] The dc current-voltage characteristics of the individual devices were measured as a function of magnetic field in a top-loading dilution refrigerator at the base temperature of $T=23$ mK.

Submicrometer-diameter DBRTS's exhibit, in addition to the vertical double-barrier confinement of large-area devices, a lateral confinement which is ideally due to mid-band-gap Fermi-level pinning at the pillar sidewalls,[2] but in reality often enhanced by the presence of impurities in the dot region or by potential fluctuations from the heavily doped contacts.[9,10] Hence, a quantum dot results with discrete spectra of 0D (zero-dimensional) states of which we denote the ground-state energies by $E(N)$. In spite of the sidewall confinement, the electron states in the contacts are in our case more 3D- than 1D-like, since the potential-fluctuation width exceeds the 1D-subband spacing. For zero bias the quantum dot is empty because the ground-state energy $E(1)$ of the first electron [equal to the charging energy $\mu(1)$] lies above the chemical potentials $\mu_{E,C}^{ch}$ of the emitter and collector contact, respectively [Fig. 1(a), left]. Upon applying a bias between emitter (negative polarity) and collector (grounded), $\mu(1)$ is reduced with respect to the electrochemical potential $\mu_E=-eV+\mu_E^{ch}$ of the emitter until the energies match and the first electron tunnels into the quantum dot [Fig. 1(a), right]. Since the electron subsequently leaves the dot through the collector barrier, a single-electron tunneling current $\Delta I=(e/\hbar)T_E\mu_E^{ch}T_CE_0/(T_E\mu_E^{ch}+T_CE_0)$ results (with $T_{E,C}$ the emitter- and collector-barrier transmission coefficients and E_0 the resonant 2D subband energy of large-area DBRTS's).[4] If μ_E exceeds the N-electron charging energy

$$\mu(N)=E(N)-E(N-1), \qquad (1)$$

up to N electrons can simultaneously occupy the quantum dot. We consider the case in which the collector barrier is much thicker than the emitter barrier ($T_E\gg T_C$). If an electron leaves the quantum dot through the collector barrier, another one enters rapidly through the high-transmission emitter barrier. Therefore, the electron number in the dot has for $\mu(N)\leq\mu_E<\mu(N+1)$ the maximum energetically allowed value N most of the time (it is lower only for a fraction of time of the order of $T_C/T_E\ll1$). As tunneling current results the product of electron number and single-electron current $I(N)=N\Delta I$. Additional emitter channels into excited N-electron states do not considerably change the current for

 © 1995 The American Physical Society

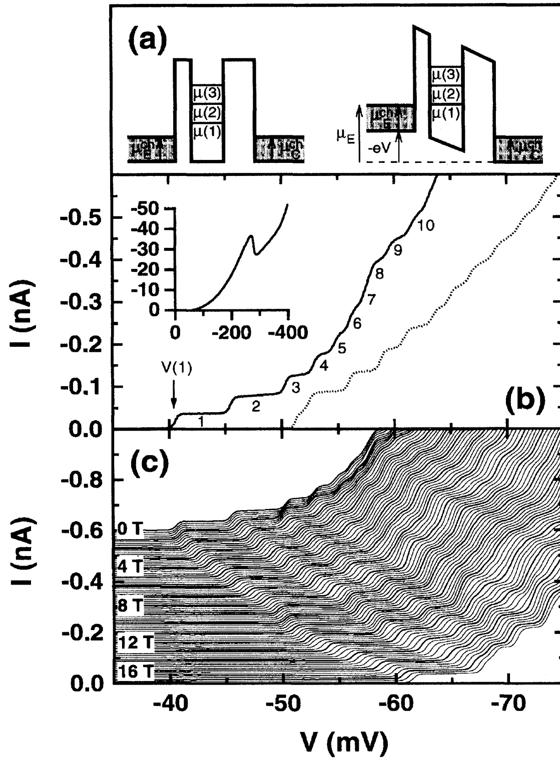

FIG. 1. (a) Schematic energy diagrams of a submicrometer-diameter DBRTS for $V=0$ and threshold bias $V=V(1)$ (space-charge layers are omitted for clarity). (b) $I(V)$ staircase of a 350-nm-diameter sample showing current steps due to single-electron charging. The inset depicts the $I(V)$ characteristics up to higher bias. The dashed line corresponds to a different device of equal size. (c) Magnetic-field dependence of the $I(V)$ staircase. The curves are plotted with a vertical offset (step 0.2 T).

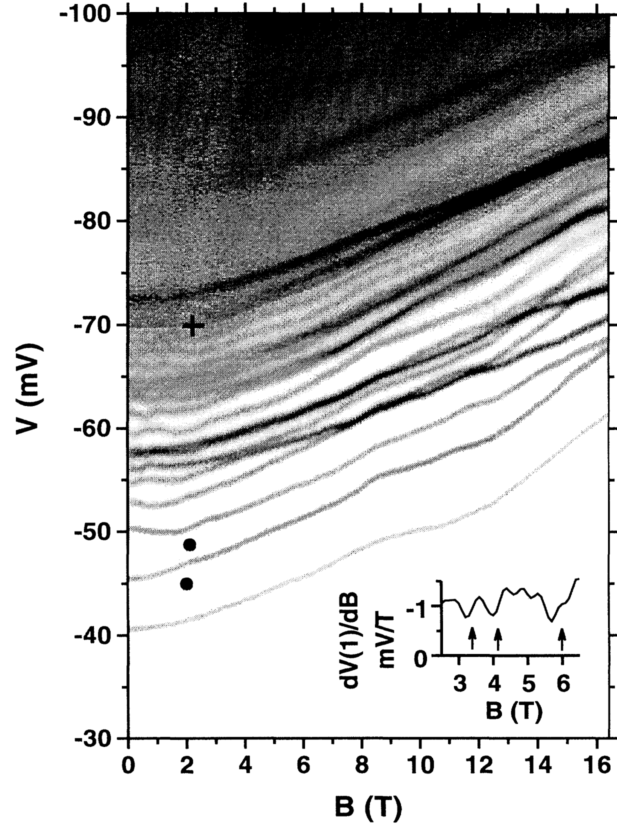

FIG. 2. Gray-scale plot of the differential conductance $G = dI/dV$ vs bias voltage and magnetic field (step 0.1 T), numerically obtained from the $I(V)$ data (white, $G \leqslant 0.01$ μS; black, $G \geqslant 0.15$ μS). The inset shows the derivative of the first conductance resonance with respect to the magnetic field. Annotations are explained in the text.

$T_E \gg T_C$ since the current is determined by tunneling through the collector barrier. Thus, single-electron charging of the quantum dot leads to a *current-voltage staircase* $I(V)$. The bias positions of the current steps

$$V(N) = \mu(N)/e\alpha \qquad (2)$$

provide, according to Eq. (1), direct experimental access to the N-electron ground-state energies $E(N)$ starting from $N=1$ (α denotes the voltage-to-energy conversion coefficient).

Figure 1(b) shows the low-bias $I(V)$ characteristics of a strongly asymmetric DBRTS with pillar diameter $d_p \approx 350$ nm (solid line). A staircaselike curve with current steps of almost equal height and smooth plateaus is observed beyond the current threshold. Incremental charging of the quantum dot with up to 10 electrons can be clearly resolved. The height of the first current step is in reasonable agreement with the theoretically obtained value of $\Delta I = 60$ pA. Both the slight inclination of the current plateaus and the small systematic increase of the current-step heights are attributed to the increasing transmission probability through the barriers with growing bias. In comparison with the work of Su *et al.*,[4] our data show no fine structure superimposed on the plateaus, since, as a consequence of the very large asymmetry, emitter density of states fluctuations have no significant impact on the tunneling current [T_E/T_C has for our design at bias $V(1)$ a value as high as 200 which exceeds that for the DBRTS of Ref. 4 by two orders of magnitude]. The inset depicts the $I(V)$ curve over an extended voltage range. We estimate a conducting diameter of $d_e = 240$ nm from comparison of the resonant-tunneling peak current with large-area devices assuming a diameter-independent current density. This value is consistent with the pillar diameter $d_p \approx 350$ nm considering a sidewall-depletion length of 50 nm due to mid-gap Fermi-level pinning. The dashed line shows the $I(V)$ staircase of another 350-nm-diameter DBRTS. Its first current step is a double step with strongly reduced plateau width in comparison with the following steps. This indicates the charging of two separate spatial regions inside the dot that are energetically lowered with respect to the bottom of the sidewall-confinement potential. For the rest of the paper, we focus on the device with the solid $I(V)$ curve which shows an even smaller threshold bias $V(1)$, suggesting transport through one low-energy region localized within the pillar. Magnetotunneling measurements prove this assessment as discussed in the following.

The influence of a magnetic field B on the current-step bias positions $V(N)$ is twofold: It affects first the many-electron ground-state energies $E(N)$ and, hence, the charging

energies $\mu(N)$ as well as second the chemical potentials $\mu_{E,C}^{ch}$ of the contacts. The resonance-bias positions vary with magnetic field as

$$e\alpha\Delta V(N) = \Delta\mu(N) - \Delta\mu_E^{ch}. \qquad (3)$$

Figure 1(c) shows the $I(V)$ staircase as a function of magnetic field oriented parallel to the current direction. The magnetic field provides an additional lateral confinement and thus shifts all current steps in a similar way to higher bias, while the current-step heights are not significantly influenced in the few-electron regime.

The gray-scale plot Fig. 2 depicts the differential conductance $G = dI/dV$ as a function of bias voltage and magnetic field. The conductance resonance $V(1) = E(1)/e\alpha$ of the *first electron* is, in the low-field region up to $B = 3$ T, well described by assuming a two-dimensional parabolic confinement potential[11] $V(r) = \frac{1}{2}m^* \omega_0^2 r^2$ with $\hbar\omega_0 = 3.6$ meV [$\alpha = 0.44$ as calculated with a self-consistent Poisson solver at bias $V(1)$]. From the classical turning points of the ground state we deduce $d_c = 2\sqrt{2\hbar/m^*\omega_0} \approx 50$ nm as confinement length, which is considerably smaller than the conducting diameter $d_e = 240$ nm but larger than twice the Bohr radius of GaAs. This demonstrates that neither lateral sidewall confinement nor single impurities in the quantum dot provide the lowest-lying electron states. Instead a natural quantum dot is formed inside the fabricated quantum pillar. This low-energy region originates either from growth-induced fluctuations of the quantum-well width (2 meV potential variation per monolayer), from potential fluctuations due to the deliberately doped contact regions (standard deviation in the quantum dot of about 1 meV), or, most probably, from donors segregated unintentionally into the spacer or barrier layers during sample growth. The width of the first plateau of the $I(V)$ staircase is estimated in complete neglect of lateral quantization using a simple electrostatic parallel plate-capacitor model. We find $V(2) - V(1) = (e^2/C_\Sigma)/e\alpha = 9$ meV, which exceeds the experimental value of 5 meV considerably (with $C_\Sigma \approx 2[\epsilon\epsilon_0\pi(d_c/2)^2/b]$ the total capacitance of the quantum dot, $b \approx 10$ nm the effective barrier thickness, $\epsilon = 11.4$). This indicates that the confinement strength decreases rapidly with increasing energy (increasing electron number in the dot) as the disorder-induced potential is gradually replaced by the sidewall confinement.

Oscillatory features are superimposed on the conductance resonance $V(1)$ in Fig. 2 (more clearly visible in the derivative shown by the inset, see the arrows). According to Eq. (3) dips occur in the conductance resonances, whenever the chemical potential attains a maximum, i.e., whenever an *emitter Landau band* is depopulated. Such dips are shown by $V(1)$ at $B \approx 3.4$, 4.2, 6.0 and 11.5 T. Since these deviations are rather periodic in $1/B$ and, moreover, particularly the last one is present in all resolved resonances, they indeed originate from oscillations of the chemical potential in the emitter. The transition to the magnetic quantum limit in which only one Landau band remains populated occurs at $B \approx 11.5$ T. We estimate an electron density of $(\sqrt{2}/\pi^2)(eB/\hbar)^{3/2} = 3.3 \times 10^{17}$ cm^{-3} assuming purely 3D spin-degenerate emitter states.[12] This value compares well with the local electron density 2.7×10^{17} cm^{-3} close to the emitter barrier as obtained from the self-consistent Poisson solver.

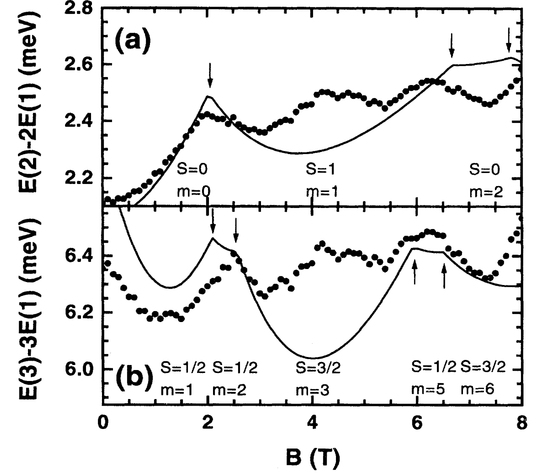

FIG. 3. Comparison of the experimental data (solid circles) for $E(2) - 2E(1)$ (a) and $E(3) - 3E(1)$ (b) with results obtained from an exact diagonalization of the few-electron Hamiltonian (solid lines). The numbers give the total electron spin S and azimutal quantum number m for two (a) and three electrons (b).

The conductance resonances in the *few-electron* regime exhibit additional structure absent in $V(1)$, which is particularly evident at $B \approx 2$ T in $V(2)$ and $V(3)$ (marked by dots in Fig. 2). A comparison with the results of an exact diagonalization of the few-particle Hamiltonian for $1 \leq N \leq 3$ relates these features to angular momentum transitions of the ground states $E(2)$ and $E(3)$. The calculation describes the quantum dot as a 2D disk whose Hamiltonian considers the electron-electron interaction via unscreened Coulomb potentials in addition to the kinetic energy, parabolic confinement-potential, and Zeeman terms.[6] The value of $\hbar\omega_0$ is taken from the observed magnetic-field dependence of $E(1)$. In order to separate the nontrivial magnetic-field dependences of $E(2)$ and $E(3)$, we consider in Figs. 3(a) and 3(b) the following bias-voltage differences [Eqs. (1) and (2)]:

$$E(2) - 2E(1) = e\alpha[V(2) - V(1)],$$

$$E(3) - 3E(1) = e\alpha[V(3) + V(2) - 2V(1)].$$

In addition, the emitter influence drops out of both expressions [Eq. (3)]. The theoretical curves are classified according to the total electron spin S and azimuthal quantum number m of $E(2)$ and $E(3)$, respectively.[13] They are, moreover, shifted along the energy axis since the charging energies that result numerically are too large for $B = 0$ T (by about a factor two). Concerning $E(2) - 2E(1)$, we identify the experimentally observed sharp peak at $B = 2.0$ T with a spin-singlet to triplet transition [Fig. 3(a)]. The calculated double-peak structure of $E(3) - 3E(1)$ at $B = 2.1$ T and 2.5 T is not separately resolved in the experimental data [Fig. 3(b)]. Further experimental features present in both $E(2) - 2E(1)$ and $E(3) - 3E(1)$ near $B = 4$ T and 6 T seem related to spin transitions predicted theoretically at higher field. When comparing our theoretical and experimental results, we have to keep in mind that the model completely neglects the screening of the intradot electron-electron interaction by the high-density electron gas of the contact regions (which are only

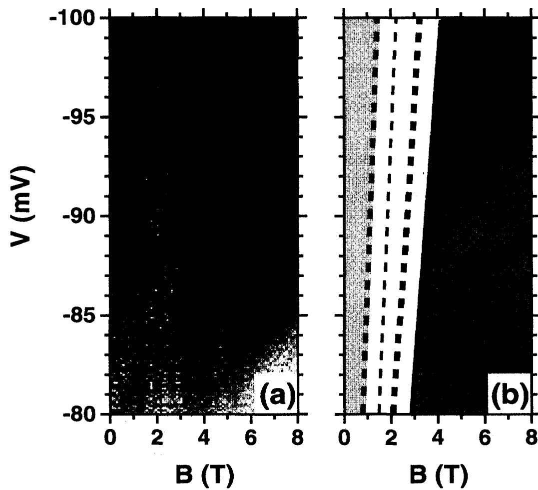

FIG. 4. (a) Low magnetic-field and many-electron regime of the differential conductance data (magnified from Fig. 2; white, $G \leqslant 0.06$ μS; black, $G \geqslant 0.13$ μS). (b) Sketch of the main features visible in (a). Black dashed lines mark local maxima in a region of reduced conductance.

about 10 nm away from the quantum dot). A smaller interaction leads to reduced charging energies (in accordance with the experimental data) but also shifts the angular momentum transitions to even higher magnetic fields (in contradiction to the experimental results). The most critical point is, however, the assumption of parabolic confinement, since the actual confinement strength decreases with increasing electron number in the dot. Reduced confinement shifts the angular momentum transitions to lower fields (in agreement with the experimental observations). Recent efforts to model the capacitance data of Ashoori *et al.*[5] met similar problems as ours: Either the magnetic-field position of the first spin singlet-triplet crossing of $E(2)$,[7] the magnetic-field dependence of $E(1)$,[14] or even both criteria[6] are not compatible with the experimental data. Moreover, the calculated charging energies are also too large.

In the *many-electron* regime ($N \geqslant 30$) clear resonances are no longer observable in the differential conductance [Fig. 4(a)]. However, a region with reduced conductance evolves at low magnetic fields, which is interrupted by three local maxima. For clarity the main structures of Fig. 4(a) are sketched in Fig. 4(b). Recently Palacios *et al.*[7] predicted a strong correlation-induced reduction of the tunneling rate if the Landau-level filling factor of the dot is in the regime $1<\nu<2$. Using $\nu=1$ for the abrupt increase following the conductance depression, we obtain $d_\nu = 2\sqrt{N(h/\pi eB\nu)} \approx 200$ nm as dot diameter (for $N=17$ and corresponding magnetic field $B \approx 2.2$ T, marked by a cross in Fig. 2). This value compares well with the conducting diameter $d_e = 240$ nm of the device, which indicates that the disorder-induced low-energy regions of the quantum dot are almost completely filled with electrons. Applying the electrostatic parallel plate-capacitor model, we estimate for $d_\nu = 200$ nm a current-plateau width of 0.6 mV which is less than the width of the conductance resonances in Fig. 2 and, thus, explains why these are no longer resolved at high bias voltage.

The most intricate case in our experiment is the regime of *intermediate electron numbers* in the quantum dot ($5 \leqslant N \leqslant 15$) since the disorder-induced potential fluctuations are gradually smoothed and replaced by the fabrication-induced sidewall confinement as the low-energy regions become filled with electrons. Here, some curves show a slightly weaker magnetic-field dependence than others whose curvature is similar to that of $V(1)$ (Fig. 2). Hence, different conductance resonances cross each other. These features are attributed to independent charging of local potential minima which are higher lying and yet more strongly localized than the already partially filled dot region of lowest energy. At present we lack a quantitative understanding of this transition regime, since the particular spatial distribution of the fluctuating potential is unknown.

In summary, we employed single-electron tunneling spectroscopy to study the ground-state energies of a strongly asymmetric, vertically etched quantum dot as a function of electron number and magnetic field. Landau-band depopulation oscillations of the chemical potential in the emitter, angular-momentum transitions of the few-electron ground states as well as correlation-induced tunneling-rate modulations in the many-electron regime were observed.

We thank V. I. Fal'ko, F. Stern, and J. Weis for continuous stimulating discussions as well as P. Grambow and B. Schönherr for expert reactive-ion etching. This work was funded by the Bundesministerium für Forschung und Technologie.

---

*Present address: Deutsche Bank, Taunusanlage 12, 60325 Frankfurt, Germany.

[1] For a review see *Single Charge Tunneling—Coulomb Blockade Phenomena in Nanostructures*, Vol. 294 of *NATO Advanced Study Institute, Series B: Physics*, edited by H. Grabert and M. H. Devoret (Plenum Press, New York, 1992).

[2] M. A. Reed *et al.*, Phys. Rev. Lett. **60**, 535 (1988).

[3] M. Tewordt *et al.*, J. Phys. Condens. Matter **2**, 8969 (1990).

[4] B. Su *et al.*, Phys. Rev. B **46**, 7644 (1992).

[5] R. C. Ashoori *et al.*, Phys. Rev. Lett. **71**, 613 (1993).

[6] P. Hawrylak, Phys. Rev. Lett. **71**, 3347 (1993).

[7] J. J. Palacios *et al.*, Phys. Rev. B **50**, 5760 (1994).

[8] P. Grambow *et al.*, Microelectron. Eng. **11**, 47 (1990).

[9] M. W. Dellow *et al.*, Phys. Rev. Lett. **68**, 1754 (1992); J. W. Sakai *et al.*, Appl. Phys. Lett. **64**, 2563 (1994); A. K. Geim *et al.*, Phys. Rev. B **50**, 8074 (1994).

[10] M. Tewordt *et al.*, Phys. Rev. B **46**, 3951 (1992).

[11] V. Fock, Z. Phys. **47**, 446 (1928).

[12] Tunneling from 2D emitter states is negligible due to the narrow spacer and, hence, small emitter accumulation layer.

[13] In a narrow magnetic-field regime beyond $B=6.5$ T the three-electron ground state (quadruplet) is not available by adding one electron to the two-electron ground state (singlet) due to spin conservation.

[14] F. Bolton, Solid State Electron. **37**, 1159 (1994).

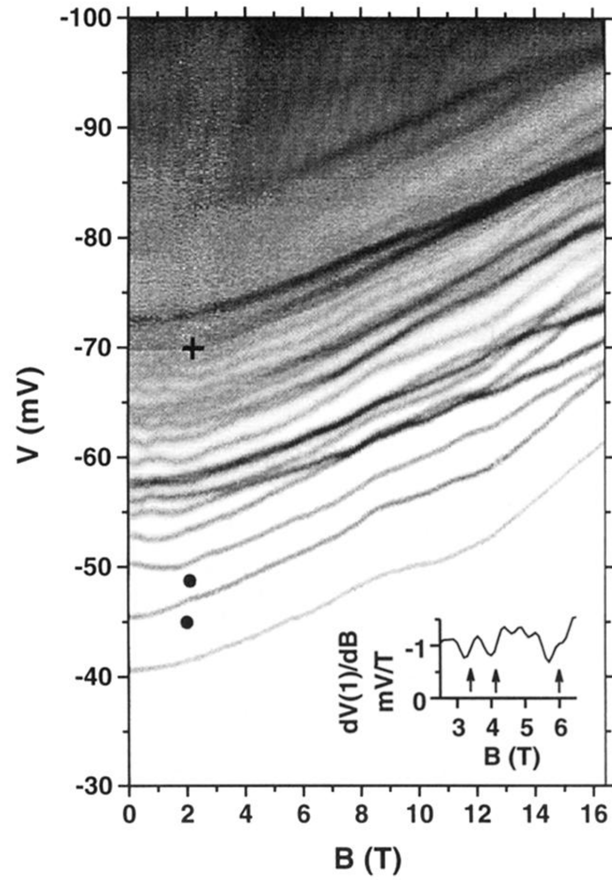

FIG. 2. Gray-scale plot of the differential conductance $G = dI/dV$ vs bias voltage and magnetic field (step 0.1 T), numerically obtained from the $I(V)$ data (white, $G \leqslant 0.01$ μS; black, $G \geqslant 0.15$ μS). The inset shows the derivative of the first conductance resonance with respect to the magnetic field. Annotations are explained in the text.

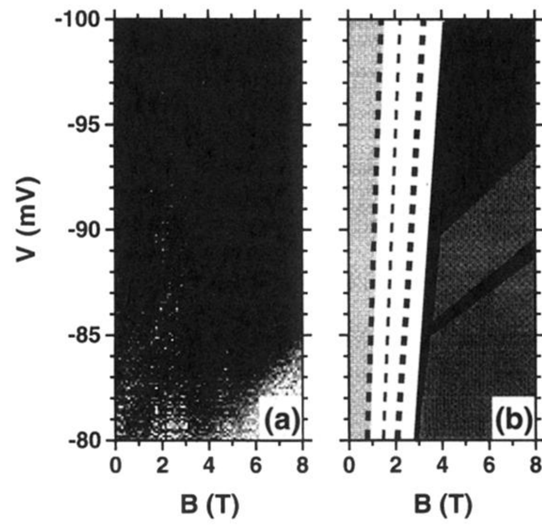

FIG. 4. (a) Low magnetic-field and many-electron regime of the differential conductance data (magnified from Fig. 2; white, $G \leqslant 0.06\ \mu\mathrm{S}$; black, $G \geqslant 0.13\ \mu\mathrm{S}$). (b) Sketch of the main features visible in (a). Black dashed lines mark local maxima in a region of reduced conductance.